New Repetitive Control with Improved Steady-state Performance and Accelerated Transient

Xu Chen and Masayoshi Tomizuka

UNIVERSITY OF CALIFORNIA, BERKELEY

Emails: maxchen@berkeley.edu, tomizuka@me.berkeley.edu

March 10, 2013

Abstract

In repetitive control, the enhanced servo performance at multiple repetitive frequencies is usually followed by undesired error amplifications at other frequencies. This report presents a new structural configuration of the internal model principle in repetitive control, wherein designers have more flexibility in the repetitive loop-shaping design, and the amplification of non-repetitive errors can be largely reduced. The algorithm applies to both regulation and tracking controls. Compared to conventional repetitive control, the proposed scheme is especially advantageous when the repetitive task is subject to large amounts of non-periodic disturbances. An additional benefit is that the transient response of the plug-in repetitive control can be easily controlled, leading to an accelerated transient with reduced overshoots. Verification of the algorithm is provided by simulation and experiment results on a hard disk drive system and a laboratory testbed of an industrial wafer stage.

Contents

List of Figures

Chapter 1

Introduction

Repetitive control (RC) is a well-known servo design tool for systems that are subjected to periodic disturbances/references. It implements an internal model (Francis and Wonham, 1975) $1/\left(1-z^{-N}\right)$ (N is the period the disturbance/reference), or $1/\left(1-e^{-T_p s}\right)$ in the continuous-time domain (T_p denotes the period), into a feedback system, such that errors in the previous periods can be used to improve the current regulation/tracking control. Distinguished by its high performance as well as the simple design and implementation criteria, ever since its introduction (T. Inoue and Baba, 1981; Hara et al., 1988; Tomizuka et al., 1989), RC has attracted a great amount of research efforts (Hillerström and Walgama, 1996; Li et al., 2004; Hara et al., 1988; Tomizuka et al., 1989). Its versatility has been tested in various practical applications, including but not limited to: track-following in magnetic and optical disk drives (Chew and Tomizuka, 1990; Kempf et al., 1993; Moon et al., 2002; Onuki and Ishioka, 2000; Guo, 2002), robot arm control (Cosner et al., 1990; Tsao and Tomizuka, 1994), and regulation control in vehicles (Longman, 2000). For more complete lists of applications, readers can refer to the survey papers (Hillerström and Walgama, 1996; Li et al., 2004).

The configuration of the internal model and its interaction with the feedback system vary in literature. The continuous-time RC design mainly applies a series or parallel plug-in configuration (Moon et al., 2002; Doh et al., 2006; Hara et al., 1988; Inoue, 1990; Srinivasan and Shaw, 1990; Tsai and Yao, 2002). The prototype RC (Tomizuka et al., 1989; Tomizuka, 2008) applies the Zero-Phase-Error-Tracking (Tomizuka, 1987) idea and directly cascades a robust version of $1/\left(1-z^{-N}\right)$ into the open-loop transfer function. Additionally there are plug-in configurations of discrete RC design, among

which (Steinbuch et al., 2007; Pipeleers et al., 2008) applied optimization techniques with an extended high-order internal model.

Ultimately, a generalized version of $1-z^{-N}$ or $1-e^{-T_p s}$ is absorbed into the denominator of the overall feedback controller, therefore creating high-gain control near the repetitive frequencies (frequencies of the roots of $1-z^{-N}=0$ or $1-e^{-T_p s}=0$). From the Bode's Integral Theorem (see, e.g., Doyle et al. (1992)), enhanced servo performance at certain frequencies commonly results in deteriorated loop shapes at other frequencies. This fundamental limitation, reflected in repetitive control, is the comb-like magnitude response in the closed-loop sensitivity function, along with undesired gain amplifications at frequencies other than the comb centers (see some examples in Moon et al. (2002); Doh et al. (2006); Srinivasan and Shaw (1990); Tsai and Yao (2002); Steinbuch et al. (2007); Pipeleers et al. (2008)). The problem is more significant if there are large non-periodic components in the disturbance (e.g., in hard disk drive systems (Ehrlich and Curran, 1999)).

Relaxing the previous performance limitations, this report proposes a new structural RC design with greatly improved loop-shaping properties. In this first contribution of the report, we provide an approach to extract only the repetitive errors, and introduce the notion of a repetitive disturbance observer (RDOB) as a new RC tool. In the frequency domain, this corresponds to a series-parallel implementation of the internal model with direct control of comb-like loop shape, leading to greatly reduced gain amplifications at the non-repetitive frequencies. An additional advantage of the reduced gain amplification is that the proposed design shows increased ability to reject repetitive errors at higher frequencies. A second contribution of the report is to provide a generalized concept of the disturbance observer (DOB) (Ohnishi, 1993), which has been well-known as a robust control design tool (Kempf and Kobayashi, 1999; White et al., 2000; Eom et al., 2001; Tan et al., 2003; Bohn et al., 2004; Yang et al., 2005) but, to the authors' best knowledge, has not been discussed in a general context for repetitive control. Finally, the new structural configuration provides a flexible control of the transient performance in RC, leading to a smoother and accelerated transient response.

The remainder of the report is organized as follows. Chapters 2 and 4 present the proposed controller design and the stability conditions. Chapter 3 provides a detailed comparison of the proposed algorithm with the prior arts. In Chapter 5, we discuss the reduction of overshoot and transient time when turning on the compensator. Chapter 6 provides verification of the algorithm by simulation and

experimentation. Chapter 7 concludes the report.

Chapter 2

Controller parametrization

Fig. 2.1 presents the proposed closed-loop repetitive control scheme. Here $P\left(z^{-1}\right)$ is the sampled plant (with digital holders) to be controlled. $C\left(z^{-1}\right)$ is the baseline controller designed by any proper loop-shaping methods to achieve the baseline servo performance and robustness. The signals $r(k)$, $y(k)$, $u(k)$, and $d(k)$ are respectively the reference, the plant output, the control input, and the lumped input disturbance. The block diagram applies to regulation as well as tracking control. In the former case, $r(k) = 0$, and the control aim is to reduce the error $e(k)$ in the presence of the disturbance $d(k)$. In the latter, $r(k)$ has a much larger magnitude than $d(k)$, and it is aimed at maintaining $e(k)$ small w.r.t. a non-zero $r(k)$.

The proposed plug-in RC design utilizes the internal signals $e(k)$ and $u(k)$ to generate a compensation signal $c(k)$. In the intermediate filtering process in Fig. 2.1, m denotes the relative degree of $P\left(z^{-1}\right)$; $P_n^{-1}\left(z^{-1}\right)$ is a nominal model of $z^{-m}P^{-1}\left(z^{-1}\right)$; and $Q\left(z^{-1}\right)$ is a filter to be designed shortly. Notice that $P^{-1}\left(z^{-1}\right)$ may be anti-causal but we have added delays such that $P_n^{-1}\left(z^{-1}\right)$ is realizable in Fig. 2.1.

Notice that if the $P_n^{-1}\left(z^{-1}\right)$ block is removed from Fig. 2.1 and $Q\left(z^{-1}\right)$ is set to $z^{-(N-m)}$, the open-loop transfer function becomes $P\left(z^{-1}\right)\frac{1}{1-z^{-N}}C\left(z^{-1}\right)$, and the proposed compensator reduces to a plug-in repetitive controller that is similar to prior arts. To see the intuition of the proposed construction and the new configuration of $Q\left(z^{-1}\right)$, we first transform the block diagram to a repetitive disturbance observer (RDOB) scheme. Notice that for either regulation or tracking, RC aims at maintaining $e(k)$ small. Relocating $e(k)$ to the right-hand side of the block diagram, extending

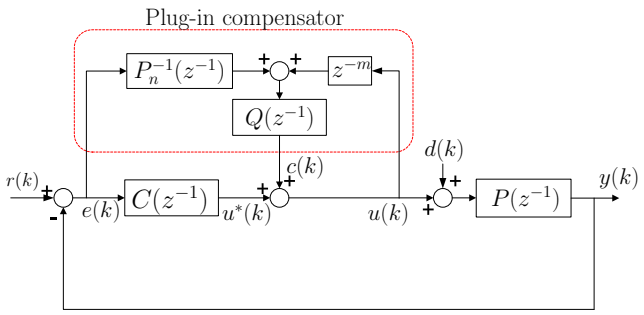

Figure 2.1: Block diagram of the proposed repetitive control scheme.

the line that connects $C\left(z^{-1}\right)$ and $P_n^{-1}\left(z^{-1}\right)$, and changing the signs of signals without altering the overall transfer functions, one obtains a unified regulation problem in Fig. 2.2, where $-e\left(k\right)$ can be regarded as a fictitious output that is regulated in the presence of the equivalent disturbances $d\left(k\right)$ and $r\left(k\right)$. For simplicity, assume first $r\left(k\right)=0$ (the case for rejecting repetitive disturbances). Since $y\left(k\right)=P\left(z^{-1}\right)\left(u\left(k\right)+d\left(k\right)\right)$, the output of $P_n^{-1}\left(z^{-1}\right)$ is given by $P_n^{-1}\left(z^{-1}\right)P\left(z^{-1}\right)\left(d\left(k\right)+u\left(k\right)\right)$. Notice that $P_n^{-1}\left(z^{-1}\right)\approx z^{-m}P^{-1}\left(z^{-1}\right)$. Through the inverse filtering, the $P_n^{-1}\left(z^{-1}\right)$ block thus approximately generates $u\left(k-m\right)+d\left(k-m\right)$. Subtracting now $u\left(k-m\right)$, the output of the z^{-m} block, yields an approximated $d\left(k-m\right)$ (i.e., $u_Q\left(k\right)=\hat{d}\left(k-m\right)$). Due to the m-step delay, the non-repetitive components in $d\left(k\right)$, and the unavoidable modeling errors in $P_n^{-1}\left(z^{-1}\right)$, $\hat{d}\left(k-m\right)$ should not be directly applied to cancel $d\left(k\right)$. The idea of the proposed RDOB is to first obtain this estimated $d\left(k-m\right)$ via the preceding filtering and then apply a Q filter that aims at extracting only the repetitive components and counteracting the m-step delay effect. This intuition applies also to the case when $r\left(k\right)\neq 0$ (in repetitive reference tracking), where the output of $Q(z^{-1})$ is an approximation of $-P^{-1}\left(z^{-1}\right)r\left(k\right)$.

Fig. 2.2 differs from conventional DOB-based servo control (see, e.g., Lee and Tomizuka (1996); Eom et al. (2001); Tan et al. (2003)) in two aspects. First, the reference signal is injected before the $P_n^{-1}\left(z^{-1}\right)$ block rather than at the summing junction before $C\left(z^{-1}\right)$. Second, $Q\left(z^{-1}\right)$ is a customized repetitive signal extractor rather than a lowpass filter. The first point transforms a reference tracking problem to a regulation problem, while the second contributes to form a repetitive-control scheme.

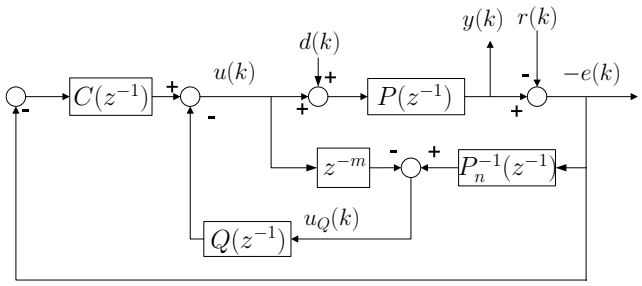

Figure 2.2: Equivalent scheme of Fig. 2.1, from the perspective of a disturbance observer.

2.1 Repetitive loop shaping

One can show from Fig. 2.1, that the equivalent controller from $e(k)$ to $u(k)$ is

$$C_{eq}\left(z^{-1}\right) = \frac{C\left(z^{-1}\right) + Q\left(z^{-1}\right) P_n^{-1}\left(z^{-1}\right)}{1 - z^{-m} Q\left(z^{-1}\right)}, \tag{2.1}$$

from which one can obtain the sensitivity function $S = 1/\left(1 + PC_{eq}\right)$ (for simplicity, we omit the z-domain index z^{-1} here):

$$S = \frac{1 - z^{-m} Q}{1 + PC + \left(PP_n^{-1} - z^{-m}\right) Q}. \tag{2.2}$$

The transfer functions from $d(k)$ and $r(k)$ to $e(k)$ are respectively given by

$$G_{ed}\left(z^{-1}\right) = P\left(z^{-1}\right) S\left(z^{-1}\right) \tag{2.3}$$

$$G_{er}\left(z^{-1}\right) = -S\left(z^{-1}\right). \tag{2.4}$$

Notice that in regions where the frequency response $P\left(e^{-j\omega}\right)$ is well modeled by $e^{-jm\omega} P_n\left(e^{-j\omega}\right)$, the contribution of $\left[P\left(z^{-1}\right) P_n^{-1}\left(z^{-1}\right) - z^{-m}\right] Q\left(z^{-1}\right)$ in (2.2) is small (in the frequency domain). In the frequency regions where large model mismatch exists, we will make $Q\left(e^{-j\omega}\right)$ small such that the denominator of (2.2) is still close to $1 + P(z^{-1})C(z^{-1})$. By the above constructions,

$$S \approx \frac{1 - z^{-m} Q\left(z^{-1}\right)}{1 + P\left(z^{-1}\right) C\left(z^{-1}\right)} \tag{2.5}$$

and one can focus on designing the term $1 - z^{-m} Q\left(z^{-1}\right)$ to introduce the desired regulation/tracking performance to the closed-loop system.

Assume $r(k)$ and $d(k)$ contain only repetitive components that satisfy the internal model[1]

$$\left(1-z^{-N}\right) r(k)=0,\ \left(1-z^{-N}\right) d(k)=0. \tag{2.6}$$

From (2.3) and (2.4), to reject $d(k)$ and $r(k)$, it suffices to have $S\left(z^{-1}\right) d(k)$ and $S\left(z^{-1}\right) r(k)$ converge asymptotically to zero. By combining (2.2) and (2.6), one may notice that this sufficient condition is achieved if $1-z^{-m}Q\left(z^{-1}\right)$ contains the term $1-z^{-N}$. In this report we propose to apply an Infinite Impulse Response (IIR) filter $Q\left(z^{-1}\right) \triangleq \frac{B_Q\left(z^{-1}\right)}{A_Q\left(z^{-1}\right)}$, with the following constraint:

$$A_Q\left(z^{-1}\right)-z^{-m}B_Q\left(z^{-1}\right)=1-z^{-N}. \tag{2.7}$$

Designing

$$A_Q\left(z^{-1}\right)=1-\alpha^N z^{-N} \tag{2.8}$$

and solving (2.7) yield

$$B_Q\left(z^{-1}\right)=\left(1-\alpha^N\right) z^{-(N-m)} \tag{2.9}$$

$$1-z^{-m}Q\left(z^{-1}\right)=\frac{1-z^{-N}}{1-\alpha^N z^{-N}}. \tag{2.10}$$

Here $\alpha\,(\in(0,1))$ is the ratio between magnitudes of the poles and the zeros in $1-z^{-m}Q\left(z^{-1}\right)$, and acts as a tuning parameter during loop shaping. If $\alpha=0$, $Q\left(z^{-1}\right)$ becomes a Finite Impulse Response (FIR) filter ($Q(z^{-1})=z^{-N+m}$) and RDOB generates similar loop shapes as prior arts. This will be discussed in more details in Chapter 3. On the other hand, $\alpha=1$ cuts off the repetitive compensation. When $\alpha\in(0,1)$, the loop shape can be flexibly designed. For instance, let $N=10$, $m=1$, and assume a sampling frequency of 26400 Hz. Increasing α from 0 to 0.99 yields the magnitude responses in Fig. 2.3. One observes from the top plot that, as α increases towards 1, $1-z^{-m}Q\left(z^{-1}\right)$ has a sharper comb-like magnitude response, and a smaller H_∞ norm. Correspondingly in the bottom plot, $Q\left(z^{-1}\right)$ behaves as a sharper spectral selection filter to preserve only the repetitive components. Specifically, if $\alpha=0$ (the case corresponding to conventional RC), $Q\left(z^{-1}\right)$ has a magnitude response valued always

[1]Since tracking and regulation are usually separate problems, we consider here a common period for $r(k)$ and $d(k)$.

at 1, losing the spectral selection property; in the mean time, the maximum value of $1-z^{-m}Q\left(z^{-1}\right)$ equals $\left\|1-z^{-m}z^{-(N-m)}\right\|_{\infty}=2$, almost twice of the value in the case of $\alpha=0.99$. One can observe that the design of (2.8) and the introduction of α have provided an additional degree of freedom for repetitive loop shaping, enabling the improvement in Fig. 2.3, from the solid lines to the dash-dotted lines. Indeed, we have the following theorem:

Theorem 1. *When $P\left(z^{-1}\right)=z^{-m}P_n\left(z^{-1}\right)$, for non-repetitive disturbances that does not satisfy $d(k)=d(k-N)$, conventional RC amplifies the disturbance by 100% in the worst case. The amplification is at most by $\left(2/\left(1+\alpha^N\right)-1\right)\times 100\%$ in RDOB. The maximum amplification occurs to the disturbance components at the frequencies $\frac{(2k+1)\pi}{2\pi T_s N}$, $k=0,1,\ldots$.*

Proof. The maximum disturbance amplification corresponds to the maximum magnitude response of $1-z^{-m}Q(z^{-1})$ in (2.2). For (2.10), the squared magnitude response is

$$\frac{1-e^{-j\omega N}}{1-\alpha^N e^{-j\omega N}}\times\frac{1-e^{j\omega N}}{1-\alpha^N e^{j\omega N}}=\frac{1-\cos(\omega N)}{\frac{1+\alpha^{2N}}{2}-\alpha^N\cos(\omega N)}, \tag{2.11}$$

where $\omega=2\pi\Omega_{Hz}T_s$ (Ω_{Hz} is in Hz, T_s is the sampling time in sec).

Noting, $\cos(\omega N)\in[-1,1]$, we need only consider the function

$$f(x)=\frac{1-x}{\frac{1+\alpha^{2N}}{2}-\alpha^N x},\ x\in[-1,1].$$

The derivative of $f(x)$ is

$$f'(x)=\frac{-\frac{1}{2}\left(1-\alpha^N\right)^2}{\left(\frac{1+\alpha^{2N}}{2}-\alpha^N x\right)^2},\ x\in[-1,1].$$

It is straightforward to see that $f'(x)$ monotonically decreases as x increases from -1 to 1. Thus, $\max\{f(x)\}$ and $\min\{f(x)\}$ are attained respectively at $x=-1$ and $x=1$, with $\min\{f(x)\}=0$ and

$$\max\{f(x)\}=\left(\frac{2}{1+\alpha^N}\right)^2. \tag{2.12}$$

Note (2.11) is the squared magnitude response. Taking the square root of (2.12) gives the maximum amplification gain of RDOB, at the frequencies $\Omega_{Hz}=\frac{(2k+1)\pi}{2\pi T_s N}$, $k=0,1,\ldots$ (the solutions of

$x = \cos(2\pi\Omega_{Hz}T_sN) = -1$). As a special case of $\alpha = 0$ (conventional RC), $\max\{f(x)\} = 4$, which indicates $\left\|1 - z^{-m}Q(z^{-1})\right\|_\infty = 2$, i.e., non-repetitive disturbance gets amplified by 100% at the computed frequencies Ω_{Hz}'s. □

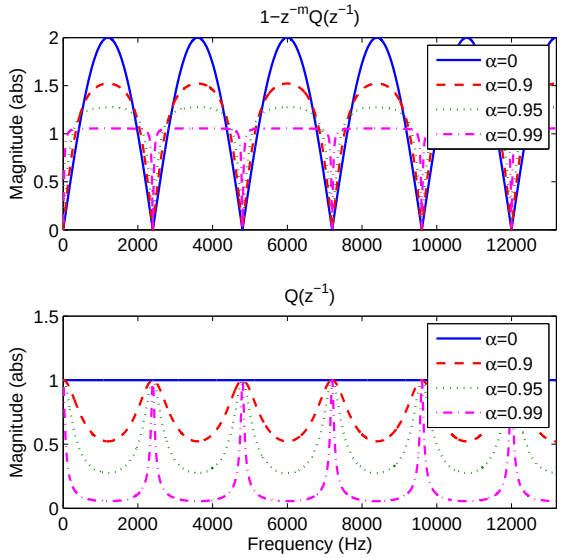

Figure 2.3: Magnitude responses of $1 - z^{-m}Q\left(z^{-1}\right)$ and $Q\left(z^{-1}\right)$ with different values of α.

2.2 Robustness and the implementation of $Q\left(z^{-1}\right)$

One central assumption in the previous subsection is the small gain of $\left[P\left(z^{-1}\right)P_n^{-1}\left(z^{-1}\right) - z^{-m}\right]Q\left(z^{-1}\right)$ in (2.2). It is practically not possible to have an accurate model of $P\left(z^{-1}\right)$ in the high-frequency region, and thus necessary to incorporate a lowpass filter in $Q\left(z^{-1}\right)$. In the context of repetitive control, it is additionally possible to apply a zero-phase lowpass filter. One simple and flexible construction is proposed as follows. Define first the following zero-phase lowpass filter as a base structure

$$q_0\left(z, z^{-1}\right) = \frac{(1+z^{-1})^{n_0}(1+z)^{n_0}}{4^{n_0}}, \tag{2.13}$$

where $2n_0$ is the number of placed zeros at the Nyquist frequency. To have additional freedom on the cut-off frequency, one can add extra zero-phase pairs given by

$$q_i\left(z,z^{-1}\right) = q_i\left(z^{-1}\right) q_i\left(z\right), \tag{2.14}$$

$$q_i\left(z^{-1}\right) = \frac{1+2\cos\left(\omega_i T_s\right) z^{-1} + z^{-2}}{2+2\cos\left(\omega_i T_s\right)}. \tag{2.15}$$

Here i is the index number; ω_i is in rad/sec. The filter $q_i\left(z,z^{-1}\right)$ places four zeros to annihilate the input spectra at at $e^{\pm\omega_i T_s}$, and is normalized by $\left(2+2\cos\left(\omega_i T_s\right)\right)^2$ to have a unity DC gain. The zero-phase property is preserved since the frequency responses of $q_i\left(z^{-1}\right)$ and $q_i\left(z\right)$ are complex conjugates of each other.

One can then define $q\left(z,z^{-1}\right) = \prod_j q_j\left(z,z^{-1}\right)$, and construct the practical version of $Q\left(z^{-1}\right)$:

$$Q\left(z^{-1}\right) = \frac{\left(1-\alpha^N\right) z^{-\left(N-m-n_q\right)}}{1-\alpha^N z^{-N}} z^{-n_q} q\left(z,z^{-1}\right), \tag{2.16}$$

where n_q is the highest order of z in $q\left(z,z^{-1}\right)$ (so that $z^{-n_q} q\left(z,z^{-1}\right)$ is realizable). One can note that $Q\left(z^{-1}\right)$ is causal as long as $N-m-n_q \geq 0$. Fig. 2.4 presents one realization of (2.16), with N memory elements for the repetitive signal generator. The bandwidth of the lowpass filter $q\left(z,z^{-1}\right)$ can roughly be tuned by comparing the magnitude responses of $\left[P\left(z^{-1}\right) P_n^{-1}\left(z^{-1}\right) - z^{-m}\right] Q\left(z^{-1}\right)$ and $1+P\left(z^{-1}\right) C\left(z^{-1}\right)$. A more strict constraint from the stability criteria will be provided in Chapter 4.

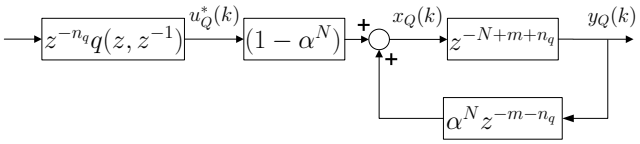

Figure 2.4: Implementation of the Q filter.

2.3 The plant and its inverse

In Fig. 2.1, stability of $P_n^{-1}\left(z^{-1}\right)$ is required for internal stability. If $P_n\left(z^{-1}\right)$ is a minimum-phase system, $P_n^{-1}\left(z^{-1}\right)$ can directly be used. For a practical sampled-data system, non-minimum phase zeros may occur in $P\left(z^{-1}\right)$ (usually in the high-frequency region (Astrom et al., 1984; Skogestad and

Postlethwaite, 2005)). If this happens, the Zero-Phase-Error-Tracking (ZPET) algorithm (Tomizuka, 1987) can be used to obtain a stable $P_n^{-1}\left(z^{-1}\right)$.

An additional concern for $P\left(z^{-1}\right)$ is the possible appearance of resonances in the high-frequency region. Modeling the resonances in $P_n\left(z^{-1}\right)$ renders a high-order $P_n\left(z^{-1}\right)$ while considering them as uncertainties yields a more conservative design. In this case, one can extend $P\left(z^{-1}\right)$ to include the baseline anti-resonance controllers (e.g., notch filters), yet with a possible increase of m in $P_n^{-1}\left(z^{-1}\right) \approx z^{-m}P^{-1}\left(z^{-1}\right)$, due to the phase loss in anti-resonance design.

Chapter 3

Connections with prior arts

With (2.16), the equivalent feedback controller in (2.1) is

$$C_{eq} = \frac{q\left(z,z^{-1}\right)\left(1-\alpha^N\right)z^{-(N-m)}P_n^{-1} + \left(1-\alpha^N z^{-N}\right)C}{1-\left[1-\left(1-\alpha^N\right)\left(1-q\left(z,z^{-1}\right)\right)\right]z^{-N}}.$$

For the ideal case of $q\left(z,z^{-1}\right)=1$ (perfect disturbance rejection),

$$C_{eq} = \left[\left(1-\alpha^N\right)z^{-(N-m)}P_n^{-1} + \left(1-\alpha^N z^{-N}\right)C\right] / \left(1-z^{-N}\right).$$

One can remark that the internal model is absorbed in the loop in a series-parallel fashion (the two terms in the numerator of C_{eq} are in parallel form, and the common part $1/(1-z^{-N})$ is in series with them).

Table 3.1 summarizes the equivalent overall feedback controllers in different repetitive control schemes. The reference of the related algorithms are as follows:

- RDOB w/ an IIR Q: the present report
- RDOB w/ an FIR Q: the present report
- Prototype RC: Tomizuka et al. (1989); Tomizuka (2008)
- Plug-in RC: Moon et al. (2002); Doh et al. (2006); Inoue (1990); Srinivasan and Shaw (1990); Tsai and Yao (2002); Dotsch et al. (1995); Hara et al. (1988)

- High-order RC Steinbuch et al. (2007); Pipeleers et al. (2008)

The ideal forms in the second and the third columns provide perfect disturbance rejection but are highly sensitivity to model mismatches. Lowpass filters in the form of $q(z,z^{-1})$ or $q(s)$ are used in the robust versions. $C\left(z^{-1}\right)$ and $C(s)$ denote the baseline feedback controllers. On the fourth line of Table 3.1, $P_{ZPET}^{-1}\left(z^{-1}\right)$ in prototype RC denotes the ZPET inverse (Tomizuka, 1987) that approximates $P^{-1}\left(z^{-1}\right)$.

Several connections can be made from Table 3.1. First, comparing "Prototype RC" with "RDOB with an FIR Q", one can observe that the former can be regarded as a special case of $C\left(z^{-1}\right)=0$ and $z^{m}P_{n}^{-1}\left(z^{-1}\right)=P_{ZPET}^{-1}\left(z^{-1}\right)$ in RDOB with an FIR Q filter. Second, if one replaces z^{-N} with $\sum_{m} w_{m}z^{-mN}$, then the high-order RC can be realized in a similar fashion as RDOB with an FIR Q filter. Third, a frequent choice of $F(s)$ in Plug-in RC is simply to have $F(s)=1$. In this case the prototype RC can be regarded as the discrete-time version of a special plug-in RC with $C(s)=P^{-1}(s)$.

It can now be seen that with an *FIR* Q filter, the proposed RDOB has close connections with prior arts. From the second and the third rows of Table 3.1, an IIR Q provides a different integration of the internal model and introduces the additional design freedom of α. This is the advantage of the proposed algorithm to surpass the previous performance limitations.

Table 3.1: Equivalent feedback controllers in repetitive control schemes

	Ideal form	(expanded) Ideal form	Robust version
RDOB w/ an IIR Q	$\frac{C(z^{-1})+P_n^{-1}(z^{-1})Q(z^{-1})}{1-z^{-m}Q(z^{-1})}$, $Q(z^{-1})=\frac{(1-\alpha^N)z^{-N+m}}{1-\alpha^N z^{-N}}$	$\frac{(1-\alpha^N)z^{-(N-m)}P_n^{-1}(z^{-1})+(1-\alpha^N z^{-N})C(z^{-1})}{1-z^{-N}}$	$\frac{q(z,z^{-1})(1-\alpha^N)z^{-(N-m)}P_n^{-1}(z^{-1})+(1-\alpha^N z^{-N})C(z^{-1})}{1-[1-(1-\alpha^N)(1-q(z,z^{-1}))]z^{-N}}$
RDOB w/ an FIR Q	$\frac{C(z^{-1})+P_n^{-1}(z^{-1})Q(z^{-1})}{1-z^{-m}Q(z^{-1})}$, $Q(z^{-1})=z^{-N+m}$	$\frac{z^{-(N-m)}P_n^{-1}(z^{-1})+C(z^{-1})}{1-z^{-N}}$	$\frac{q(z,z^{-1})z^{-(N-m)}P_n^{-1}(z^{-1})+C(z^{-1})}{1-q(z,z^{-1})z^{-N}}$
Prototype RC	$\frac{k_r z^{-N}}{1-z^{-N}}P_{ZPET}^{-1}(z^{-1})$, $k_r\in(0,2)$	$\frac{k_r z^{-N}}{1-z^{-N}}P_{ZPET}^{-1}(z^{-1})$	$\frac{k_r q(z,z^{-1})z^{-N}}{1-q(z,z^{-1})z^{-N}}P_{ZPET}^{-1}(z^{-1})$
Plug-in RC	$C(s)\left(1+F(s)\frac{e^{-T_p s}}{1-e^{-T_p s}}\right)$, $F(s)$ differs in specific papers.	$C(s)\frac{(1-e^{-T_p s})+F(s)e^{-T_p s}}{1-e^{-T_p s}}$	$C(s)\frac{(1-q(s)\cdot e^{-T_p s})+q(s)F(s)\cdot e^{-T_p s}}{1-q(s)\cdot e^{-T_p s}}$
High-order RC	$\frac{C(z^{-1})T_n^{-1}(z^{-1})\sum_m w_m z^{-mN}}{1-\sum_m w_m z^{-mN}}$, $T_n\approx\frac{P(z^{-1})C(z^{-1})}{1+P(z^{-1})C(z^{-1})}$	$\frac{(P^{-1}(z^{-1})+C(z^{-1}))\sum_m w_m z^{-mN}}{1-\sum_m w_m z^{-mN}}$	$\frac{C(z^{-1})T_n^{-1}(z^{-1})(\sum_m w_m z^{-mN})q(z,z^{-1})}{1-(\sum_m w_m z^{-mN})q(z,z^{-1})}$

Chapter 4

Stability and robust stability

From the previous discussions, if $P_n^{-1}\left(z^{-1}\right)$ and $Q\left(z^{-1}\right)$ are properly designed, the sensitivity function in (2.2) approximates $\frac{1-z^{-m}Q}{1+PC}$, and the closed-loop stability is preserved. Strict nominal closed-loop stability is obtained by using (2.1) and computing the roots of the characteristics equation from $1+P\left(z^{-1}\right)C_{eq}\left(z^{-1}\right)=0$.

When the plant is perturbed to be $\tilde{P}\left(z^{-1}\right)=P\left(z^{-1}\right)\left(1+\Delta\left(z^{-1}\right)\right)$ (assume the uncertainty $\Delta\left(z^{-1}\right)$ is stable and has a bounded H_∞ norm), applying the Small Gain Theorem (see, e.g., Doyle et al. (1992)) yields the following robust-stability condition:

$$\left\|\Delta\left(z^{-1}\right)T\left(z^{-1}\right)\right\|_\infty < 1, \tag{4.1}$$

where the complementary sensitivity function $T=\frac{PC_{eq}}{1+PC_{eq}}$ is given by, after simplification,

$$T=\frac{CP+P_n^{-1}PQ}{1+CP+Q\left(P_n^{-1}P-z^{-m}\right)}.$$

Notice that to avoid conservativeness, we perturbed the plant w.r.t. $P\left(z^{-1}\right)$ instead of $z^{-m}P_n\left(z^{-1}\right)$, since from Chapter 2.3 the latter term may already contain reduced information compared to $P\left(z^{-1}\right)$.

Chapter 5

Transient response

With the plug-in compensator, a new feedback system is formed. The plug-in repetitive controller may be turned on or off depending on the presence of repetitive disturbances. Although the two closed loops are designed to be asymptotically stable, switching between the two stabilizing controllers in general does not yield smooth response (Liberzon and Morse, 1999). To be more specific for the plug-in repetitive control, note that Fig. 2.4 has the following state-space realization

$$\begin{aligned} x_Q(k) &= \left(1-\alpha^N\right) u_Q^*(k) + \alpha^N x_Q(k-N) \\ y_Q(k) &= x_Q\left(k-N+m+n_q\right) \end{aligned}$$

where $x_Q(k) \in \mathbb{R}^{n_Q}$ (n_Q is the order of $Q\left(z^{-1}\right)$), $u_Q^*(k) \in \mathbb{R}$, and $y_Q(k) \in \mathbb{R}$.

Notice that N, the period of the repetitive disturbance/trajectory, can be large. Correspondingly, α^N can be quite small. When $x_Q(k)$ is initialized to zero, the first $N-m-n_q$ values of $y_Q(k)$ equal zero. Starting from the time instant $N-m-n_q+1$, $y_Q\left(N-m-n_q+i\right) = \left(1-\alpha^N\right) u_Q^*(i)$ for $i \in [1,N]$. At the first period of actual compensation, depending on the baseline closed-loop dynamics, the impulse of $u_Q^*(k)$ can create high-amplitude transient response in the error signal. Additionally, all the information in $u_Q^*(k)$, including the non-repetitive components, are fed back by the compensation signal $c(k)$ in Fig. 2.2, yielding mismatched cancellation for the non-periodic errors.

To reduce the possible overshoot and amplification of non-repetitive components, we can apply a time-varying α for transient improvement. It is proposed to initialize α at 1, and exponentially reduce

Table 5.1: The influence of α on the transient and the steady-state performance

value of $\alpha\,(\in[0,1])$	steady-state performance	transient overshoot	transient duration
large	small amplification of non-repetitive components	small	long
small	converse of the above	possibly large	short

it to a designed value α_{end} (from steady-state analysis), following the decay rule

$$\alpha(k+1) = \alpha_{end} - (\alpha_{end} - \alpha(k))\,\alpha_{rate}, \tag{5.1}$$

with $\alpha(0) = 1$ and the decay rate $\alpha_{rate} \in (0,1)$. Notice that when $\alpha = 1$, the Q filter is essentially turned off ($Q\left(z^{-1}\right) = 0$ in (2.16)). By the above construction, at the first period of compensation, u_Q^* is gradually (weighted by $1-\alpha^N$) released to y_Q.

As for the settling time of the Q filter, the transient duration is determined by the pole location of the filter. Let n_t denote the number of periods for the impulse response of $Q\left(z^{-1}\right)$ to reduce to $e^{-1}\,(\approx 0.368)$. From (2.16), this time constant is determined by $\left(\alpha^N\right)^{n_t} = e^{-1}$, i.e.,

$$n_t = \frac{-1}{\log \alpha^N}. \tag{5.2}$$

From (5.2), the smaller the term α^N, the shorter the settling time. In the extreme case that $\alpha = 0$, $Q\left(z^{-1}\right)$ becomes an FIR filter in (2.16), which has no pole and $\lim_{\alpha\to 0}(n_t) = 0$.

Combining the above discussion with that of Fig. 2.3, we can obtain in Table 5.1 the influence of α on various closed-loop properties. Notice the two conflicting objectives of maintaining (1) short transient duration and (2) small transient overshoot as well as good steady-state performance. Initializing α at 1 keeps the transient smooth and gradually reducing it afterward helps to accelerate the transient. Yet to maintain the steady-state performance, the final value of α should not be too small. A slightly more complicated design of α (compared to (5.1)) is to first reduce it from 1 to a middle value α_{mid} and then increase it to a final α_{end}. A detailed design example of this is provided in Chapter 6.

Chapter 6

Case studies

6.1 Application to regulation control

This section provides a design example in the track-following control of a hard disk drive (HDD) system. In this example, the disk spins at 7200 revolutions per minute (rpm), and the regulation control aims at positioning the read/write heads to follow the data tracks as precisely as possible. We implement the proposed algorithm to the HDD benchmark problem (IEEJ, Technical Commitee for Novel Nanoscale Servo Control, 2007), where the plant is a 14-order system consisting of the dynamics of the power amplifier, the voice-coil motor, and the actuator mechanics. The input and the output of the plant correspond respectively to the (weighted) force input and the position of the read/write heads (the plant has a double-integrator type system dynamics). There are 220 sectors on each disk. Thus at every revolution of the disks, 220 measurements are obtained, and the sampling frequency becomes 26400 Hz. The baseline controller is an PID controller with several notch filters. The resulting baseline feedback system has gain and phase margins respectively of 5.45 dB and 38.2 deg, and an open loop servo bandwidth of 1.19 kHz. The period of the repeatable disturbance is thus $N = 220$, at a base frequency of $7200/60 = 120$ Hz.

In the RDOB design, we model $P\left(z^{-1}\right)$ to contain the plant as well as the notch filters. Fig. 6.1 shows the frequency responses of $P\left(z^{-1}\right)$ and $z^{-m}P_n\left(z^{-1}\right)$ ($m = 2$ in this example). Since modeling errors appear after around 2 kHz, the zero-phase lowpass filter in Chapter 2.2 is designed to have a cut-off frequency of 2025 Hz, with $n_0 = 1$ in (2.13); $\omega_1 = 2\pi \times 122000$ rad/sec and $\omega_2 = 2\pi \times 8400$

rad/sec (two additional zero-phase pairs) in (2.15). In view of the large value of N, α is designed to be 0.999 to achieve good steady-state performance. Correspondingly, α^N has a value of 0.8024. α^N is directly implemented instead of α.

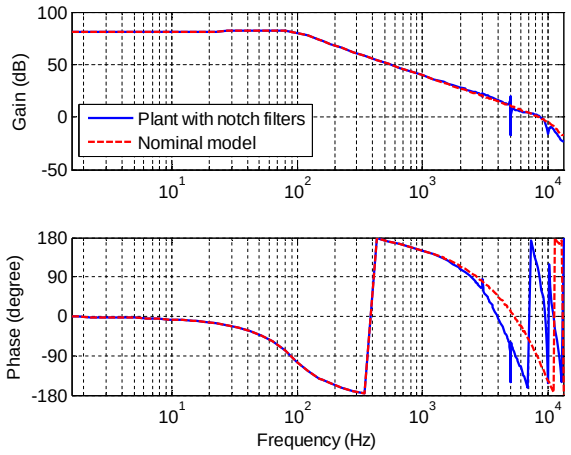

Figure 6.1: Frequency responses of $P\left(z^{-1}\right)$ and $z^{-m}P_n\left(z^{-1}\right)$.

The magnitude responses of $Q\left(z^{-1}\right)$ and $1-z^{-m}Q\left(z^{-1}\right)$ are plotted respectively in the bottom and the top plots of Fig. 6.2. Notice the repetitive spectral selection property (at multiples of the fundamental frequency 120 Hz) in $Q\left(z^{-1}\right)$. This indicates that the repetitive disturbance observer only "observes" the periodic components and filters out the non-repetitive noise in the disturbance estimation. For robustness, the zero-phase lowpass filter keeps Q-filter gain small at high frequencies, yielding the gradual reduction of compensation capacity at high frequencies in $1-z^{-m}Q\left(z^{-1}\right)$. The magnitude responses of the actual closed-loop sensitivity functions are shown in Fig. 6.3. One can see that the designed loop shape in $1-z^{-m}Q\left(z^{-1}\right)$ is successfully transformed to the closed-loop system (recall the loop-shaping criterion (2.5)), and that the frequency responses at the non-repetitive frequencies are preserved in Fig. 6.3. The loop-shaping results can be compared with those in Tsai and Yao (2002); Steinbuch et al. (2007); Srinivasan and Shaw (1990).

Fig. 6.4 shows the magnitude responses of $1/T$, the inverse of the complementary sensitivity function. From (4.1), in order to preserve the robust stability, magnitude of the plant uncertainty has to be lower than that of $1/T$ at all frequencies. From the top plot, we observe that the introduction of RDOB largely preserves the robust stability bounds (compared to the baseline closed-loop system), especially in the high-frequency region. The minimal value of the solid line is -4.7dB (0.582 in

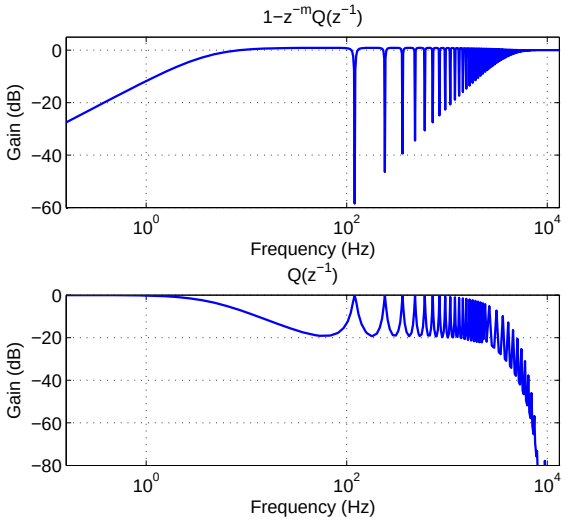

Figure 6.2: Magnitude responses of $1-z^{-m}Q\left(z^{-1}\right)$ and $Q\left(z^{-1}\right)$.

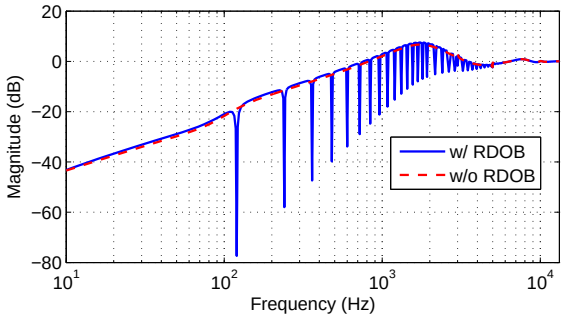

Figure 6.3: Magnitude responses of the sensitivity functions with and without RDOB.

absolute value) at 1327 Hz, i.e., the plant uncertainty should not be more than 58.2% at this frequency. The necessity of the zero-phase lowpass filter $q(z,z^{-1})$ is evident from the bottom plot. Without $q(z,z^{-1})$, 3 percent (-31dB) of model uncertainty at 6000 Hz will drive the system unstable.

Simulation is conducted by applying a full set of practical disturbances that includes the disk-flutter disturbance, the sensor noise, the repeatable runout (RRO), and the input force disturbance. Fig. 6.5 presents the spectra of the position error signals (PES) (in the steady state) with and without RDOB. One can remark that the repetitive errors below 2000 Hz are successfully removed,[1] and that amplification of other errors is visually not distinguishable. As a performance metric in HDD industry, the 3σ (σ denotes the standard deviation) value of the PES reduces from 10.77% Track Pitch (TP) to 9.30% TP, indicating a 13.6 percent improvement.

[1]The multiple spectral peaks between 800 Hz and 1300 Hz are due to the non-repetitive disk-flutter disturbances.

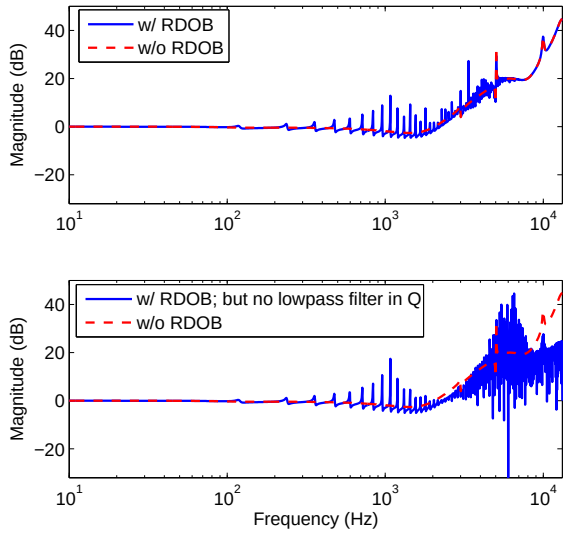

Figure 6.4: Upper bounds for the plant uncertainty for robust stability.

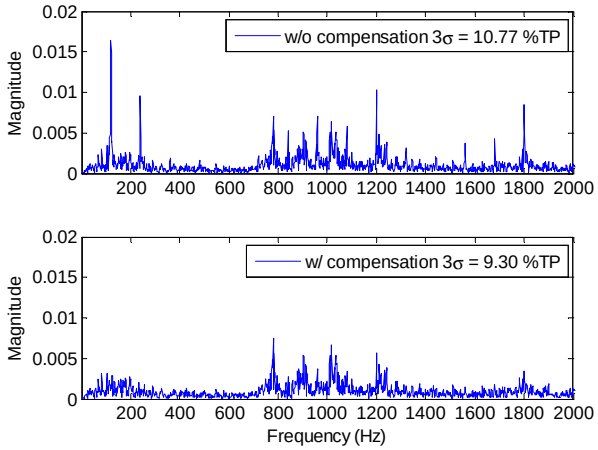

Figure 6.5: Spectra of PES with and without compensation.

The bottom plot of Fig. 6.6 shows the PES spectrum with RDOB and $\alpha = 0$, which corresponds to previous RC schemes. It is observed that the repetitive disturbance components are also significantly reduced. However, due to the amplification of the non-periodic components in-between of the repetitive frequencies (see the amplified peaks compared to Fig. 6.5, and also the enlarged view in the top plot of Fig. 6.6), the overall 3σ value does not improve but is instead amplified, as can be predicted from the steady-state loop-shaping analysis in Fig. 2.3. In addition, to avoid excessive high-frequency disturbance amplification, the bandwidth of the zero-phase lowpass filter in $Q\left(z^{-1}\right)$ has to be reduced to 1585 Hz. In this environment that consists of not only repetitive but also a significant amount of non-

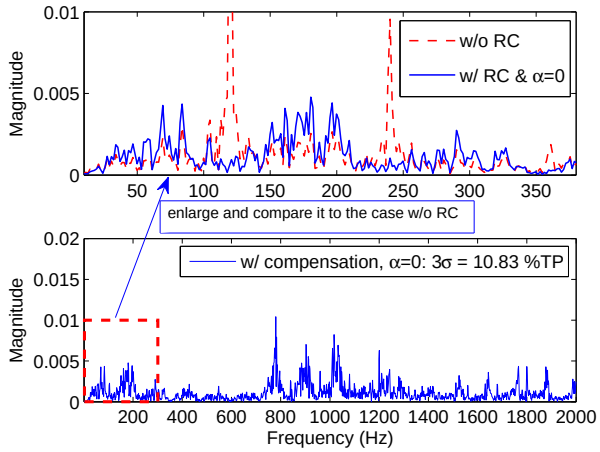

Figure 6.6: PES spectrum in RDOB with an FIR Q.

repetitive disturbances, a conventional RC has experienced difficulty improving the overall regulation performance.

To investigate further the transient performance, we provide in the following the simulation results using an additional disturbance profile that is richer in repetitive components. Figs. 6.7 and 6.8 demonstrate time traces of PES using different configurations of α in $Q\left(z^{-1}\right)$. In all cases, the baseline feedback loop has been running for 3 revolutions before RDOB is turned on. In Fig. 6.7, α maintains at 0.999 in the top plot throughout the simulation, and is configured to exponentially decay from 1 to 0.999, at the rate of 0.9/sample in the bottom plot. One can note the dynamic switching algorithm provides a much smoother transient response with no visually distinguishable overshoots.[2]

In the top plot of Fig. 6.8, the final value of the time-varying α is chosen as 0.99. One can see that a smaller α yields shorter transient response, as predicted by the analysis in Chapter 5. More specifically, the time constants (defined by (5.2)) for $\alpha = 0.999$ and 0.99 are respectively 4.5432 and 0.4523 revolutions. One can observe from Fig. 6.7 and the top plot of Fig. 6.8, that the transient durations are indeed about 4.5 and 0.5 revolutions, in agreement with what have just been computed from (5.2). Note that $\alpha = 0.99$ yields worse disturbance rejection results at the steady state. This is supported by the analysis in Chapter 2.1. One way to balance the performance is to let α first reduce quickly from 1 to 0.99, and then gradually increase to the final value 0.999. The bottom plot of Fig. 6.8 depicts the achieved PES time trace using such a configuration.

[2]The peaking phenomenon in the top plot comes from the closed-loop dynamics. By checking the dynamics of $P/(1+PC)$, one can verify that the impulse and step responses from the RDOB output to $e(k)$ have large peak values.

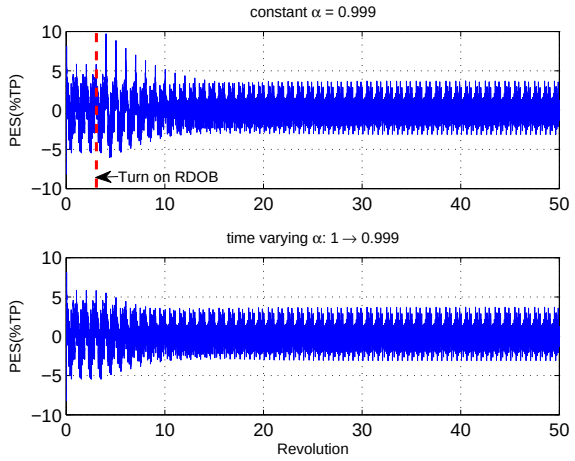

Figure 6.7: Comparison of the transient responses with and without the time-varying α in $Q\left(z^{-1}\right)$.

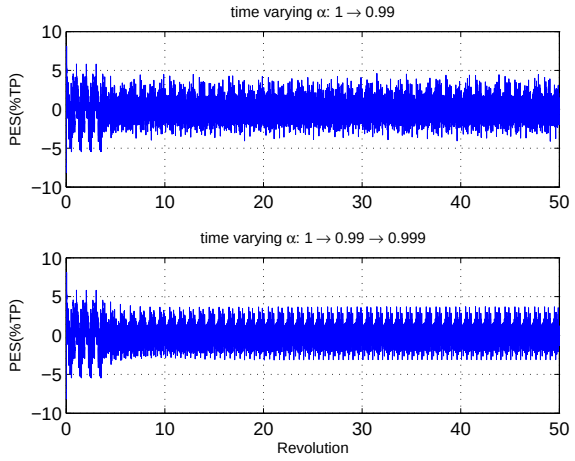

Figure 6.8: Comparison of the transient responses w.r.t. different configurations of time-varying α's.

6.2 Application to tracking control

The proposed algorithm has been implemented on a laboratory testbed of an industrial wafer stage. Such devices are essential components of wafer scanners, which are used for manufacturing integrated circuits in the semiconductor industry. The wafer stage operates by repeatedly following a designed reference trajectory. A picture of the setup is shown in Fig. 6.9. There are two stages in the system, mounted on air bearings and actuated by epoxy-core linear permanent magnet motors (LPMMs). The stage positions are measured by laser interferometers. A LabVIEW real-time system with field-programmable gate array (FPGA) is used to execute the control commands with a sampling time of 0.0004 s.

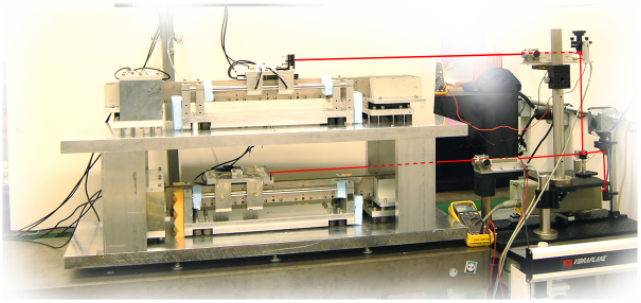

Figure 6.9: A testbed of an industrial wafer-stage system.

The top stage is used for verification of the proposed algorithm. The system has a nominal model given by

$$z^{-m}P_n\left(z^{-1}\right) = z^{-2}\frac{3.4766\times 10^{-7}(1+0.8z^{-1})}{(1-z^{-1})^2}$$

with the baseline feedback controller being a simple PID controller. The applied reference trajectory is as shown by the solid line in Fig. 6.10. The dashed line in Fig. 6.10 shows the tracking result when we applied only the baseline feedback controller. For the resulting tracking errors, the 3σ value is 3.814×10^{-4} m. The process is repetitive and the trajectory was continuously applied to the wafer stage. Fig. 6.11 presents the experimental results of the tracking errors for the first twenty repetitions, where the top and the bottom plots provide respectively the position errors without repetitive control and with the proposed algorithm. No transient control for α is applied in Fig. 6.11. One can observe that repetitive control has greatly reduced the tracking errors at the steady state. The 3σ value has reduced from 3.814×10^{-4} m at the first repetition to 4.160×10^{-6} m at the 20^{th} repetition, indicating a 99.7% reduction of 3σ. The proposed transient design algorithm is then applied to additionally accelerate the transient response. Fig. 6.12 shows the results for RDOB with transient control. Comparing the results with that in Fig. 6.11, one can see the significant reduction of transient duration while at the same time the steady-state performance has been preserved.

To compare the performance of the proposed algorithm with that of a conventional RC, a reference trajectory that consists four sinusoidal components at 20, 40, 60, and 80 Hz is tested. Additionally a random disturbance obeying a normal distribution has been applied to the system to examine the performance of the algorithms under noisy environments. The disturbance profile has been designed such that if evaluated at the injection point of the reference, the maximum magnitude of the disturbance is one half of the peak value in the reference profile. Fig. 6.13 shows the spectra of the resulting tracking

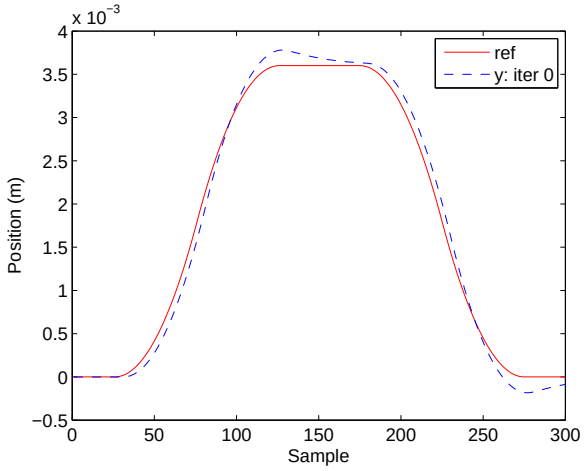

Figure 6.10: Reference trajectory and the actual wafer-stage position without repetitive control.

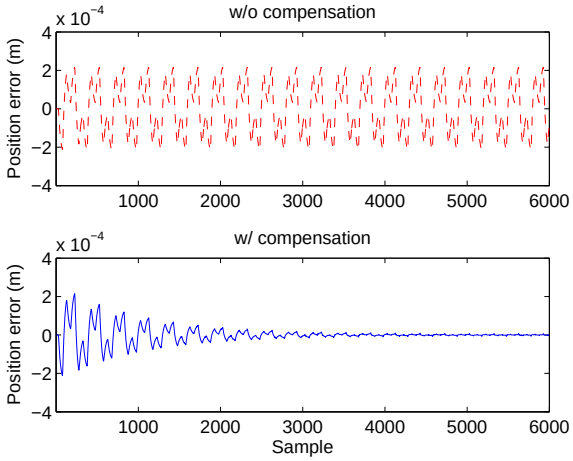

Figure 6.11: Tracking errors with RDOB but without transient control.

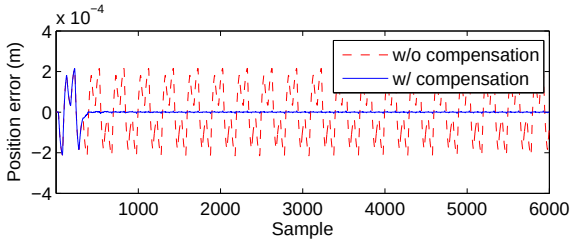

Figure 6.12: Tracking errors with RDOB and transient control.

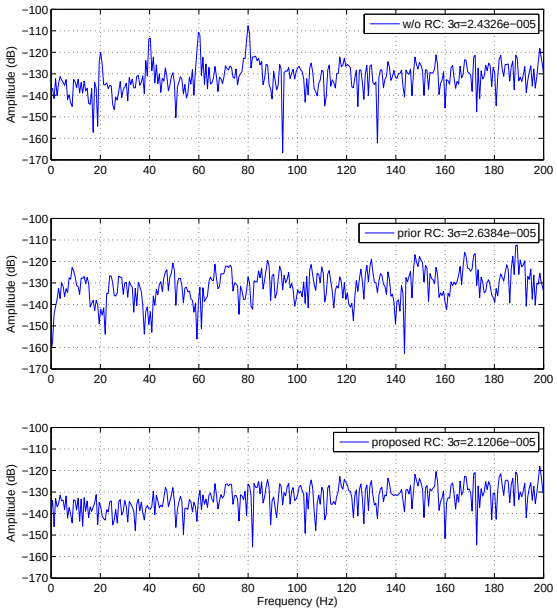

Figure 6.13: Spectra of the tracking errors under different RC schemes.

errors. It is seen from the first subplot that without repetitive control, large peaks appear at 20, 40, 60, and 80 Hz in the tracking-error spectrum. Using a conventional RC ($\alpha = 0$), spectral peaks at the repetitive frequencies are removed as shown in the middle plot. However, since conventional RC applies all the error information (including the non-periodic errors) in previous repetition, the non-repetitive errors can be seen to have increased (see the additional spectral peaks at the non-repetitive frequencies). This corresponds well to the loop-shaping results in Fig. 2.3. In the proposed scheme, only the repetitive components are reduced, and no visual amplification of the non-repetitive disturbances is observed.

Chapter 7

Conclusion

In this report, we have discussed a new repetitive control scheme using the structure of a disturbance observer. From the disturbance-observer perspective, the conventional configuration is extended to address a general class of disturbance spectrum. From the repetitive-control perspective, a series-parallel implementation of the internal model principle is proposed, with a corresponding loop-shaping design criteria that enables improved loop shapes. This has an important advantage during rejecting repetitive disturbances or following repetitive trajectories when the system is additionally subjected to non-repetitive disturbances. A dynamic switching algorithm is proposed and has been shown to effectively improve the transient performance.

Bibliography

Astrom, K., Hagander, P., Sternby, J., 1984. Zeros of sampled systems. Automatica 20 (1), 31 – 38.

Bohn, C., Cortabarria, A andHärtel, V., Kowalczyk, K., 2004. Active control of engine-induced vibrations in automotive vehicles using disturbance observer gain scheduling. Control Engineering Practice 12 (8), 1029 – 1039.

Chew, K., Tomizuka, M., 1990. Digital control of repetitive errors in disk drive systems. IEEE Control Syst. Mag. 10 (1), 16–20.

Cosner, C., Anwar, G., Tomizuka, M., May 1990. Plug in repetitive control for industrial robotic manipulators. In: Proc. 1990 IEEE International Conf. on Robotics and Automation,. pp. 1970 – 1975 vol.3.

Doh, T., Ryoo, J., Chung, M., 2006. Design of a repetitive controller: an application to the track-following servo system of optical disk drives. In: IEE Proc. Control Theory and Applications. Vol. 153. IET, pp. 323–330.

Dotsch, H., Smakman, H., Van den Hof, P., Steinbuch, M., 1995. Adaptive repetitive control of a compact disc mechanism. In: Proceedings of the 34th IEEE Conference on Decision and Control, 1995. Vol. 2. IEEE, pp. 1720–1725.

Doyle, J. C., Francis, B. A., Tannenbaum, A., 1992. Feedback control theory. Vol. 134. Macmillan.

Ehrlich, R., Curran, D., Mar 1999. Major HDD TMR sources and projected scaling with TPI. IEEE Trans. Magn. 35 (2), 885–891.

Eom, K. S., Suh, I. H., Chung, W. K., 2001. Disturbance observer based path tracking control of robot manipulator considering torque saturation. Mechatronics 11 (3), 325 – 343.

Francis, B. A., Wonham, W. M., Jun. 1975. The internal model principle for linear multivariable regulators. Applied Mathematics & Optimization 2 (2), 170–194.

Guo, L., 2002. Reducing the manufacturing costs associated with hard disk drives-a new disturbance rejection control scheme. IEEE/ASME Trans. Mechatronics 2 (2), 77–85.

Hara, S., Yamamoto, Y., Omata, T., Nakano, M., Jul 1988. Repetitive control system: a new type servo system for periodic exogenous signals. IEEE Trans. Autom. Control 33 (7), 659 –668.

Hillerström, G., Walgama, K., 1996. Repetitive control theory and applications-a survey. In: Proc. 13th IFAC World Congress. pp. 1–6.

IEEJ, Technical Commitee for Novel Nanoscale Servo Control, 2007. NSS benchmark problem of hard disk drive systems. http://mizugaki.iis.u-tokyo.ac.jp/nss/.

Inoue, T., Dec 1990. Practical repetitive control system design. In: Proc. 29th IEEE Conf. on Decision and Control. pp. 1673 –1678 vol.3.

Kempf, C., Messner, W., Tomizuka, M., Horowitz, R., Dec. 1993. Comparison of four discrete-time repetitive control algorithms. IEEE Control Syst. Mag. 13 (6), 48 –54.

Kempf, C. J., Kobayashi, S., 1999. Disturbance observer and feedforward design for a high-speed direct-drive positioning table. IEEE Trans. Control Syst. Technol. 7 (5), 513–526.

Lee, H. S., Tomizuka, M., feb 1996. Robust motion controller design for high-accuracy positioning systems. IEEE Trans. Ind. Electron. 43 (1), 48 –55.

Li, C., Zhang, D., Zhuang, X., Jan. 2004. A survey of repetitive control. In: Proc. 2004 IEEE/RSJ International Conf. on Intelligent Robots and Systems. Vol. 16. pp. 1160 – 1166.

Liberzon, D., Morse, A., 1999. Basic problems in stability and design of switched systems. IEEE Control Syst. Mag. 19 (5), 59–70.

Longman, R. W., 2000. Iterative learning control and repetitive control for engineering practice. International Journal of Control 73 (10), 930–954.

Moon, J., Lee, M., Chung, M., 2002. Repetitive control for the track-following servo system of an optical disk drive. IEEE Trans. Control Syst. Technol. 6 (5), 663–670.

Ohnishi, K., 1993. Robust motion control by disturbance observer. Journal of the Robotics Society of Japan 11 (4), 486–493.

Onuki, Y., Ishioka, H., 2000. Compensation for repeatable tracking errors in hard drives using discrete-time repetitive controllers. In: Proceedings of 6th IEEE International Workshop on Advanced Motion Control. pp. 490–495.

Pipeleers, G., Demeulenaere, B., De Schutter, J., Swevers, J., 2008. Robust high-order repetitive control: optimal performance trade-offs. Automatica 44 (10), 2628–2634.

Skogestad, S., Postlethwaite, I., 2005. Multivariable Feedback Control: Analysis and Design, 2nd Edition. Wiley Chichester, UK.

Srinivasan, K., Shaw, F.-R., May 1990. Analysis and design of repetitive control systems using the regeneration spectrum. In: Proc. American Control Conf. pp. 1150 –1155.

Steinbuch, M., Weiland, S., Singh, T., 2007. Design of noise and period-time robust high-order repetitive control, with application to optical storage. Automatica 43 (12), 2086–2095.

T. Inoue, M. Nakano, T. K. S. M., Baba, H., 1981. High accuracy control of a proton synchrotron magnet power supply. In: Proc. IFAC World Congress. pp. 3137–3142.

Tan, K. K., Lee, T. H., Dou, H. F., Chin, S. J., Zhao, S., 2003. Precision motion control with disturbance observer for pulsewidth-modulated-driven permanent-magnet linear motors. IEEE Trans. Magn. 39 (3), 1813–1818.

Tomizuka, M., 1987. Zero phase error tracking algorithm for digital control. ASME Journal of Dynamic Systems, Measurements, and Control 109 (1), 65–68.

Tomizuka, M., 2008. Dealing with periodic disturbances in controls of mechanical systems. Annual Reviews in Control 32 (2), 193 – 199.

Tomizuka, M., Tsao, T.-C., Chew, K.-K., 1989. Analysis and synthesis of discrete-time repetitive controllers. ASME Journal of Dynamic Systems, Measurement, and Control 111 (3), 353–358.

Tsai, M.-C., Yao, W.-S., jul 2002. Design of a plug-in type repetitive controller for periodic inputs. IEEE Trans. Control Syst. Technol. 10 (4), 547 –555.

Tsao, T.-C., Tomizuka, M., 1994. Robust Adaptive and Repetitive Digital Tracking Control and Application to a Hydraulic Servo for Noncircular Machining. ASME Journal of Dynamic Systems, Measurement, and Control 116 (1), 24.

White, M., Tomizuka, M., Smith, C., Mar. 2000. Improved track following in magnetic disk drives using a disturbance observer. IEEE/ASME Trans. Mechatronics 5 (1), 3–11.

Yang, K., Choi, Y., Chung, W. K., Feb. 2005. On the tracking performance improvement of optical disk drive servo systems using error-based disturbance observer. IEEE Trans. Ind. Electron. 52 (1), 270–279.